

Characterization of 7- and 19-month-old Tg2576 mice using multimodal in vivo imaging: limitations as a translatable model of Alzheimer's disease

Feng Luo^a, Nathan R. Rustay^a, Ulrich Ebert^b, Vincent P. Hradil^a, Todd B. Cole^a, Daniel A. Llano^c, Sarah R. Mudd^d, Yumin Zhang^a, Gerard B. Fox^a, Mark Day^{a,*}

^a Experimental Imaging/Advanced Technology, Global Pharmaceutical Research and Development, Abbott Laboratories, Abbott Park, IL, USA

^b CNS Discovery Research, Abbott Laboratories, Ludwigshafen, Germany

^c Neuroscience Development, Global Pharmaceutical Research and Development, Abbott Laboratories, Abbott Park, IL, USA

^d School of Pharmacy, University of Wisconsin, Madison, WI, USA

Received 12 January 2010; received in revised form 7 July 2010; accepted 9 August 2010

Abstract

With 90% of neuroscience clinical trials failing to see efficacy, there is a clear need for the development of disease biomarkers that can improve the ability to predict human Alzheimer's disease (AD) trial outcomes from animal studies. Several lines of evidence, including genetic susceptibility and disease studies, suggest the utility of fluorodeoxyglucose positron emission tomography (FDG-PET) as a potential biomarker with congruency between humans and animal models. For example, early in AD, patients present with decreased glucose metabolism in the entorhinal cortex and several regions of the brain associated with disease pathology and cognitive decline. While several of the commonly used AD mouse models fail to show all the hallmarks of the disease or the limbic to cortical trajectory, there has not been a systematic evaluation of imaging-derived biomarkers across animal models of AD, contrary to what has been achieved in recent years in the Alzheimer's Disease Neuroimaging Initiative (ADNI) (Miller, 2009). If animal AD models were found to mimic endpoints that correlate with the disease onset, progression, and relapse, then the identification of such markers in animal models could afford the field a translational tool to help bridge the preclinical-clinical gap. Using a combination of FDG-PET and functional magnetic resonance imaging (fMRI), we examined the Tg2576 mouse for global and regional measures of brain glucose metabolism at 7 and 19 months of age. In experiment 1 we observed that at younger ages, when some plaque burden and cognitive deficits have been reported, Tg2576 mice showed hypermetabolism as assessed with FDG-PET. This hypermetabolism decreased with age to levels similar to wild type (WT) counterparts such that the 19-month-old transgenic (Tg) mice did not differ from age matched WTs. In experiment 2, using cerebral blood volume (CBV) fMRI, we demonstrated that the hypermetabolism observed in Tg mice at 7 months could not be explained by changes in hemodynamic parameters as no differences were observed when compared with WTs. Taken together, these data identify brain hypermetabolism in Tg2576 mice which cannot be accounted for by changes in vascular compliance. Instead, the hypermetabolism may reflect a neuronal compensatory mechanism. Our data are discussed in the context of disease biomarker identification and target validation, suggesting little or no utility for translational based studies using Tg2576 mice.

© 2012 Elsevier Inc. All rights reserved.

Keywords: Cerebral metabolism; Hypometabolism; Hypermetabolism; FDG-PET; Functional MRI; Proton MRS; APP; Transgenic mice; Alzheimer's disease; Biomarker

1. Introduction

Alzheimer's disease (AD), a progressive neurodegenerative disease, is currently treated with acetylcholinesterase (AChE) inhibitors and N-methyl-D-aspartate (NMDA) receptor antagonists (Roberson and Mucke, 2006). Both therapies only treat symptoms and do not address the underlying

* Corresponding author at: Experimental Imaging/Advanced Technology, Global Pharmaceutical Research and Development, Abbott Laboratories R4DF, AP4-2, 100 Abbott Park Road, Abbott Park, IL 60064, USA. Tel.: +1 847 938 4266; fax: +1 847 938 5286.

E-mail address: mark.day@abbott.com (M. Day).

neurodegeneration (Roberson and Mucke, 2006). In addition to potentially improving the accuracy of diagnosis, translational medicine approaches seek to develop biomarkers in humans and animal models that can serve important roles for the development of putative disease-modifying drugs for AD (Thal et al., 2006). By providing evidence of drug activity and indirect measures of disease severity, a change in a biomarker could be considered supporting evidence of disease modification. Moreover, appropriate biomarkers will improve the predictability of drug discovery and development efforts by improving the congruency of preclinical models to clinical reality, thus establishing proof-of-concept for efficacy and safety based on targeted mechanism of action (Day et al., 2008).

There is great need for disease severity biomarkers in AD (Day et al., 2008; Thal et al., 2006). These should correlate statistically with the disease phenotypes for which therapeutics are developed. Correlation of levels or expression patterns should signify disease initiation, progression, regression, remission, or relapse (Day et al., 2008). In short they should be able to serve as a surrogate for or be superior to clinical assessments (Day et al., 2008; Thal et al., 2006). In the past decade imaging studies using magnetic resonance imaging (MRI), positron emission tomography (PET), and single photon emission computerized tomography (SPECT) have afforded major advancements in our understanding of the disease process confirming, for example, that AD follows a set limbic-cortical trajectory, with the earliest neuropathological features occurring in the entorhinal cortex, spreading into the CA1 region of the hippocampus and then neocortical regions (Norfray and Provenzale, 2004).

Whilst decreases in glucose utilization are not specific to a particular disease, over 20 years of research on brain metabolism has established that the AD brain is regionally hypometabolic even in those genetically at risk but asymptomatic (Norfray and Provenzale, 2004). In addition, decreases in fluorodeoxyglucose (FDG)-PET signals can be seen very early in the disease process. For example, healthy asymptomatic young and middle-aged individuals who carry the APOE4 gene show reductions in metabolism in brain regions affected in AD (Norfray and Provenzale, 2004; Reiman et al., 2005). Further, patients presenting with AD or mild cognitive impairment (MCI) show reductions in cerebral metabolic rates for glucose (CMRglu) in the posterior cingulate, parietal, temporal, and prefrontal cortex (Norfray and Provenzale, 2004). Moreover, this hypometabolism is correlated with dementia severity and predicts progression (Mega et al., 1997; Mosconi, 2005; Norfray and Provenzale, 2004). For example, MCI subjects who decline, compared with those that do not worsen or show spontaneous recovery, have been demonstrated to show decreased metabolism in the parietal and temporal cortex (Jagust, 2006). In MCI-AD converters, the entorhinal cortex shows a marked decrease in metabolic rate (de Leon et al., 2001; Jagust, 2006).

FDG-PET also has advantages as an outcome measure for drug trials. First, FDG-PET signals have shown pharmacological sensitivity to agents known to improve cognition in AD (Potkin et al., 2001; Teipel et al., 2006). In addition, based on longitudinal CMRglu declines in AD patients, researchers have estimated that the number of AD patients per treatment arm needed to detect an effect with FDG-PET is roughly comparable to that needed to detect an effect with volumetric MRI and almost 1 tenth the number of patients needed using clinical end points, suggesting the promise of this imaging technique in proof-of-concept trials (Alexander et al., 2002; Dickerson and Sperling, 2005). Taken together, these data suggest that changes in brain glucose utilization may serve as a disease biomarker and/or a marker for predicting drug efficacy in AD (Jagust, 2006).

Attempts to recapitulate the AD pathologies with transgenic (Tg) mice have led to several models of the disease (McGowan et al., 2006). Amyloid precursor protein (APP) Tg models display extensive plaque pathology and cognitive deficits with age (McGowan et al., 2006). One of the most widely used animal models for amyloid plaques is the Tg (HuApp695.K670N/M671L) 2576 transgenic mouse model, which overexpresses human APP with the double Swedish mutation (Hsiao et al., 1996) and are thought to reflect, in part, AD pathology, including elevated levels of amyloid beta ($A\beta$)_{1–40} and $A\beta$ _{1–42}, the presence of amyloid plaques, inflammation (Hsiao et al., 1996), as well as learning and memory deficits, herein referred to as the Tg2576 model (Hsiao et al., 1996; Irizarry et al., 1997; Jacobsen et al., 2006; Westerman et al., 2002).

In order to evaluate the Tg2576 model for cerebral glucose utilization (CGU)-based disease biomarkers, we investigated the effects of age (7 and 19 months) on CGU using in vivo [¹⁸F]-FDG-PET in experiment 1. In experiment 2, using cerebral blood volume (CBV)-based fMRI, we aimed further to determine whether there was intact vascular compliance to hypercapnia in 7-month-old Tg mice compared with wild type (WT) mice (Mueggler et al., 2002). Our results are discussed in the context of Alzheimer's disease biomarker identification and target validation.

2. Methods

2.1. Animal preparation

A total of 30 heterozygous double Swedish mutation (K670N/M671L) female Tg2576 transgenic mice expressing human APP complementary DNA (cDNA) (Hsiao, 1998; Hsiao et al., 1996; Spire and Hyman, 2005) and 30 age-matched wild type mice were employed in the study. Mice were obtained from Taconic (Germantown, NY, USA) at approximately 3 months of age but imaged at approximately 7 and 19 months of age. Different cohorts of animals were used. Mean body weights (mean \pm SD) were 23.5 ± 3.0 and 22.2 ± 4.2 g respectively for 7-month-old WT and Tg mice, and 26.5 ± 5.2 and 26.8 ± 5.4 g respectively for 19-month-

old WT and Tg mice. All mice were group housed on a filtered, forced air isolation rack, and maintained on standard sterile wood chip bedding in a quiet room under conditions of 12 hours lights on/12 hours lights off (on at 06:00), with food and water available ad libitum. An electronic chip, IMI-1000 from Bio Medical Data Systems (Seaford, DE, USA), was implanted subcutaneously in the dorsal posterior region for identification purposes. This chip was removed prior to fMRI studies. The various imaging investigations (FDG-PET, fMRI) were performed during the light phase under medetomidine (1 mg/kg intraperitoneally; Pfizer Animal Health, Exton, PA, USA) + ketamine (75 mg/kg intraperitoneally; Fort Dodge Animal Health, Fort Dodge, IA, USA) anesthesia. All experiments were conducted in accordance with Abbott Institutional Animal Care and Use Committee and National Institutes of Health Guide for Care and Use of Laboratory Animals guidelines in facilities accredited by the Association for the Assessment and Accreditation of Laboratory Animal Care.

2.2. Glucose metabolism assessment using FDG-PET

Twenty Tg2576 and 20 WT control mice were imaged using PET over 2 different age ranges: ~7 and ~19 months old. FDG-PET experiments were conducted on an Inveon PET/computed tomography (CT) (Siemens Medical Solutions USA, Inc., Knoxville, TN, USA) high resolution system dedicated to small animal imaging (microPET). The animals were fasted with free-access to water for at least 6 hours before the study. After anesthesia preparation, a tail vein catheter was inserted and the animal was placed in the imaging bed of the PET-CT system. The imaging bed extended to the PET field of view (FOV) immediately after CT image acquisition, controlled by a remote computer. PET image acquisition was initiated when a bolus of $10\text{--}15 \times 10^3$ kBq of [^{18}F]-FDG in $\sim 100 \mu\text{L}$ of saline was injected through the tail vein catheter and continued for 60 minutes. All raw PET scan data were first sorted into 3-dimensional sinograms, followed by Fourier rebinning. The dynamic PET images were framed as 1×3 seconds (s) + 12×0.5 s + 2×1.5 s + 1×16 s + 1×32 s + 1×180 s + 1×300 s + 1×460 s + 1×540 s + 1×600 s + 1×700 s + 1×760 s. Images were reconstructed iteratively using 2-dimensional (2D) ordered subset-expectation maximization reconstruction algorithm (2D-OSEM) with the following parameters: a Ramp filter with 0.5 of the Nyquist frequency as the cutoff, 5 iterations and 128×128 array size. The reconstructed CT scan was initially used for the attenuation corrections during image reconstructions, and was omitted after learning that the images without the attenuation correction provided uncompromised quantification. The energy window was set between 350 and 650 keV and brains were placed in the center of the axial FOV to minimize scattered radiation. No postacquisition scatter correction was performed. The voxel size was $0.4 \times 0.4 \times 0.8 \text{ mm}^3$. Inveon microPET radial, tangential, and axial resolutions at

center of FOV were 1.46 mm, 1.49 mm, and 1.15 mm, respectively (Constantinescu and Mukherjee, 2009).

The ordered subsets estimation algorithm (OSEM) was introduced in 1994 (Hudson and Larkin, 1994) and since that time 2D-OSEM has become the most commonly used iterative method for statistically based PET reconstruction (Leahy and Qi, 2000). Compared with traditional analytical methods such as filtered back-projection (FBP), 2D-OSEM provides improved image quality with only slightly higher computational demands. Further, for dynamic datasets with relatively low counts during early time points, the use of FBP typically results in poor image quality with high noise and low contrast. A comprehensive evaluation of OSEM reconstruction of both phantom and patient data showed that OSEM has equal quantitative accuracy as FBP and also provides improved signal-to-noise ratio that improves image resolution and reduces partial volume effects (Boellaard et al., 2001). In addition, our PET/CT scanner is calibrated regularly with known sources to ensure accurate quantification of 2D-OSEM reconstructed images.

A calibration factor for converting units on microPET images into absolute tracer concentration was first generated by imaging a Ge-68 phantom with known concentration. FDG concentration in the whole brain was quantified from each image using image analysis software from Inveon Research Workplace (Siemens Medical Solutions USA, Inc., Knoxville, TN). Brain volume was first obtained with the volume of interest (VOI) technique utilizing the CT and magnetic resonance (MR) imaging to include the entire volume inside the skull (whole brain) as well as several VOIs (hippocampus, perirhinal cortex, entorhinal cortex, striatum, thalamus, cerebral cortex, and cerebellum), which are thought to be related to AD pathology (Fig. 1). The average FDG concentrations within the brain VOI were registered and then converted into absolute concentration (kBq/cc) by the calibration factor.

Standard uptake value (SUV) was calculated as tissue tracer concentration divided by the ratio of injected dose over subject mass (grams, with the assumption 1 cc = 1 g). Although semiquantitative, SUV is a widely accepted clinical outcome for glucose utilization in neurology and oncology (see Thie, 2004 for review). Like percent injected dose (%ID)-kg/g (Klunk et al., 2005), SUV eliminated the variability in the injected doses and subject masses, facilitating comparison among animals and results from different laboratories (Klunk et al., 2005).

CT scans were performed using the Siemens Inveon preclinical scanner and Siemens Inveon Acquisition Workplace software (Version 1.0, Siemens Medical Solutions USA, Inc., Knoxville, TN, USA). Briefly, the x-ray source was set at 80 kV and $500 \mu\text{A}$ with an effective pixel size of $83 \mu\text{m}$. One hundred seventy-five projections were acquired over a 220 degree range with a total scan length of 4.3 minutes. Data were then reconstructed using a modified Feldkamp algorithm with a Shepp-Logan filter.

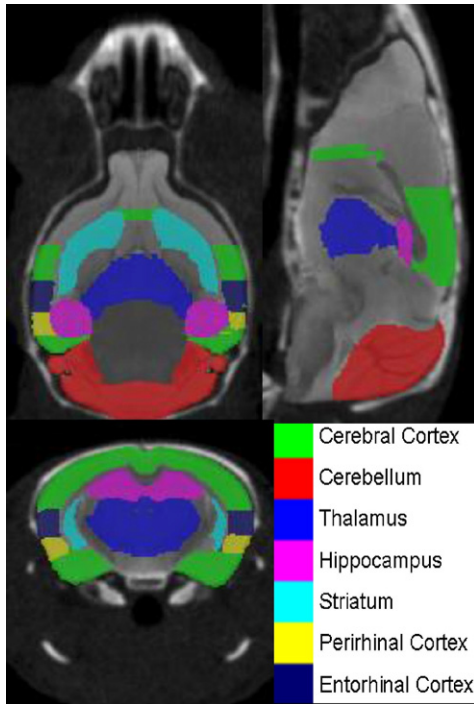


Fig. 1. Anatomical localizations of 7 volumes of interest (VOIs) from horizontal, sagittal, and coronal slices of mouse brain, according to Paxinos and Franklin stereotaxic coordinates of mouse brain. A T2-weighted magnetic resonance (MR) image (anatomical images were acquired using the fast spin-echo rapid acquisition relaxation enhanced (RARE) pulse sequence with repetition time (TR) = 3 seconds, effective echo time (TE) = 100 ms, matrix = 256×256 , field of view (FOV) = 2.56×2.56 cm, and giving an in-plane resolution = $100 \times 100 \mu\text{m}$) is fused to computerized tomography (CT) and mouse atlas. Hippocampus, perirhinal cortex, entorhinal cortex, striatum, thalamus, cerebral cortex, and cerebellum are color coded based on mouse atlas.

2.3. CBV measurement using fMRI

Acetazolamide is a well characterized carbonic anhydrase inhibitor which causes rapid increases in CBV (Vorstrup et al., 1984) by acidifying cerebral extracellular fluids through an increase in extracellular P_{CO_2} (Mueggler et al., 2002). This effect of acetazolamide on CBV can be used to assess vascular function, and is detectable in rodents via MRI (Graham et al., 1994). Ten Tg2576 and 10 WT control mice were imaged via fMRI over 2 different age ranges: ~ 7 and ~ 19 months old. A 7.0 T/21 cm horizontal magnet with a 20 G/cm magnetic field gradient insert (Bio-spec Bruker, Billerica, MA) was employed for our MRI studies. A dual-coil small animal restrainer (Insight Neuro-Imaging Systems, LLC, Worcester, MA), which contains a volume coil for transmitting and a surface coil for receiving, was used. Respiration rates and waveforms were continuously monitored via a force transducer. Rectal temperature was monitored and maintained at $37 \pm 1^\circ\text{C}$ via a feedback-regulated, circulating water pad. All imaging was performed during the light phase. Coil-to-coil electromagnetic interaction was actively decoupled. Anatomical images were ac-

quired using the fast spin-echo rapid acquisition relaxation enhanced (RARE) pulse sequence with repetition time (TR) = 3 s, effective echo time (TE) = 100 ms, matrix = 256×256 , FOV = 2.56×2.56 cm, nine 1.0-mm slices, and 4 averages. Gradient echo single-shot echo-planar imaging (EPI) was used for fMRI-CBV image acquisition with TR = 2 s, TE = 13 ms, matrix = 64×64 , FOV = 2.56×2.56 cm, and giving an in-plane resolution = $400 \times 400 \mu\text{m}$. A dose of 10 mg Fe/kg ultra small superparamagnetic iron oxide (USPIO) contrast agent (SH U555C, Schering AG, Berlin, Germany) was administered intravenously 2 minutes into an 18-minute image acquisition. Acetazolamide (30 mg/kg, intravenous) was bolus administered via the tail vein 6 minutes after the contrast agent and changes in CBV were then detected over a subsequent 10-minute period.

fMRI data analysis was performed using the Analysis of Functional NeuroImages (AFNI) software package (public license version 2, NIH, Bethesda, MD, USA, Cox, 1996). To identify time-dependent relative CBV change, $\text{CBV}(t)$, was calculated from time course raw data based on the relationship (Mandeville et al., 1998):

$$\text{CBV}(t) = \ln[s(t)/s_0(t)]/\ln[s_0(t)/s_{\text{pre}}] \quad (1)$$

where $s(t)$ is the signal intensity after acetazolamide infusion, $S_0(t)$ is the baseline signal before the acetazolamide infusion, and S_{pre} is the mean signal intensity before the administration of contrast agent. The time course CBV changes were determined with a linear function to account for elimination of contrast agent from the blood (Cox, 1996).

Subsequently, the CBV signal for each voxel in every mouse was fitted to a nonlinear differential exponential model (Eq. 2) reflecting the drug's kinetics (Luo et al., 2004; Stein, 2001) where t_0 is the time delay of response, k is the multiplicative coefficient, α_1 is the elimination rate and α_2 the absorption rate.

$$y(t) = k(e^{-\alpha_1(t-t_0)} - e^{-\alpha_2(t-t_0)}); t \geq t_0 \quad (2)$$

The initial values fitted to parameters t_0 , k , α_1 , and α_2 were 0–45 seconds, -500 – 500 , 0–0.15, and 0.15–0.5, respectively, based on known acetazolamide kinetics (Mueggler et al., 2002). Final values for t_0 , k , α_1 , and α_2 were automatically determined using AFNI based on maximal significance of model fitting (Cox, 1996).

2.4. Statistical analysis

For FDG-PET data, the VOIs were analyzed using a 2-way analysis of variance (ANOVA) model in the log scale, with the age and genotype main effects and age \times genotype interaction effect. Log transformation of the VOIs was necessary because the distribution of the original (untransformed) data were significantly nonnormal, and log transformation helped ensure adequate normality (based on the Shapiro-Wilk normality test). The age \times genotype interaction effect from this model was further evaluated to

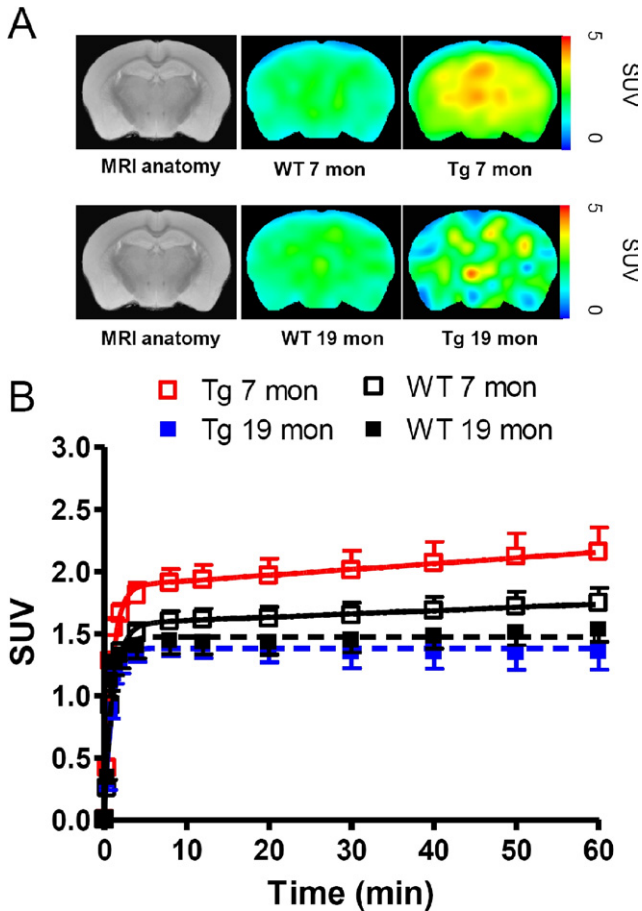


Fig. 2. Representative fluorodeoxyglucose (FDG) uptake in microPET and corresponding magnetic resonance imaging (MRI) anatomical images for wild-type (WT) and transgenic (Tg) mice at 7 months and 19 months of age (A). Group comparison of whole brain glucose metabolism between Tg and WT at 7 months and 19 months of age during time activation curve (B).

determine the significance of the genotype effect for each age, and the significance of the age effect for each strain. Statistical significance was claimed when $p < 0.05$. For

fMRI CBV data, the number of activated CBV voxels, mean amplitude CBV% change per voxel, and a response index (Luo et al., 2003) to reflect overall brain response to acetazolamide challenge ([number of activated voxels] × [average amplitude CBV% change per voxel]) were analyzed by 2-way analysis of variance (ANOVA), with age and genotype as between-group factors. Statistical significance was set at $p < 0.05$.

3. Results

A significant increase in whole brain CGU was observed in 7-month-old Tg2576 compared with age-matched WT littermates (Fig. 2A). Elevation of the time-activity curve (TAC) in brain tissue is clearly demonstrated in Tg2576 vs. WT mice minutes after the [¹⁸F]-FDG tracer was administered intravenously (Fig. 2B), although the absorption rate of the tracer did not differ significantly between Tg and age matched WT. Region-of-interest analysis revealed that CGU was significantly higher in hippocampus, perirhinal cortex, entorhinal cortex, striatum, and thalamus in 7-month-old Tg2576 compared with aged matched WT (Fig. 3). In contrast, CGU and tracer kinetics in brain in 19-month-old Tg2576 mice did not separate from aged matched WT mice (Fig. 2A and B).

The cerebral hemodynamic response to acetazolamide challenge in Tg2576 mice did not significantly differ when compared with aged-matched WT mice in terms of the number of voxels showing a CBV increase (Fig. 4B), mean amplitude changes from those activated voxels (Fig. 4C), or the calculated response index (Fig. 4D). Overall, aged mice showed fewer activated voxels ($p < 0.01$) and a lower response index ($p < 0.01$) compared with young mice, but there was no difference between genotypes. No significant impairment of vascular compliance was observed in young Tg mice, although there was a nonsignificant trend for compliance to be diminished (Fig 4D).

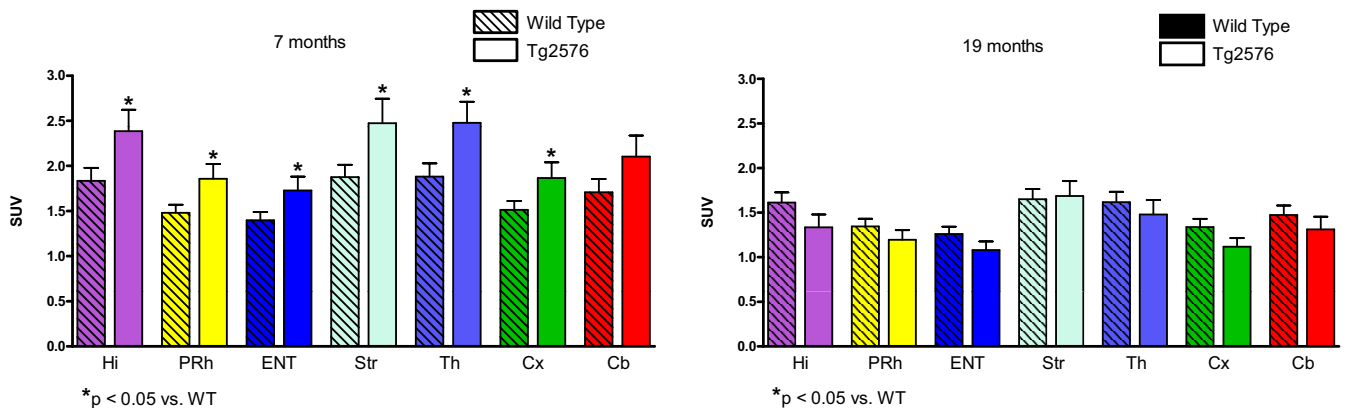


Fig. 3. Group comparison of cerebral glucose metabolism in hippocampus (Hi), perirhinal cortex (PRh), entorhinal cortex (ENT), striatum (Str), thalamus (Th), cerebral cortex (Cx), and cerebellum (Cb), between Tg and WT at 7 months and 19 months of age.

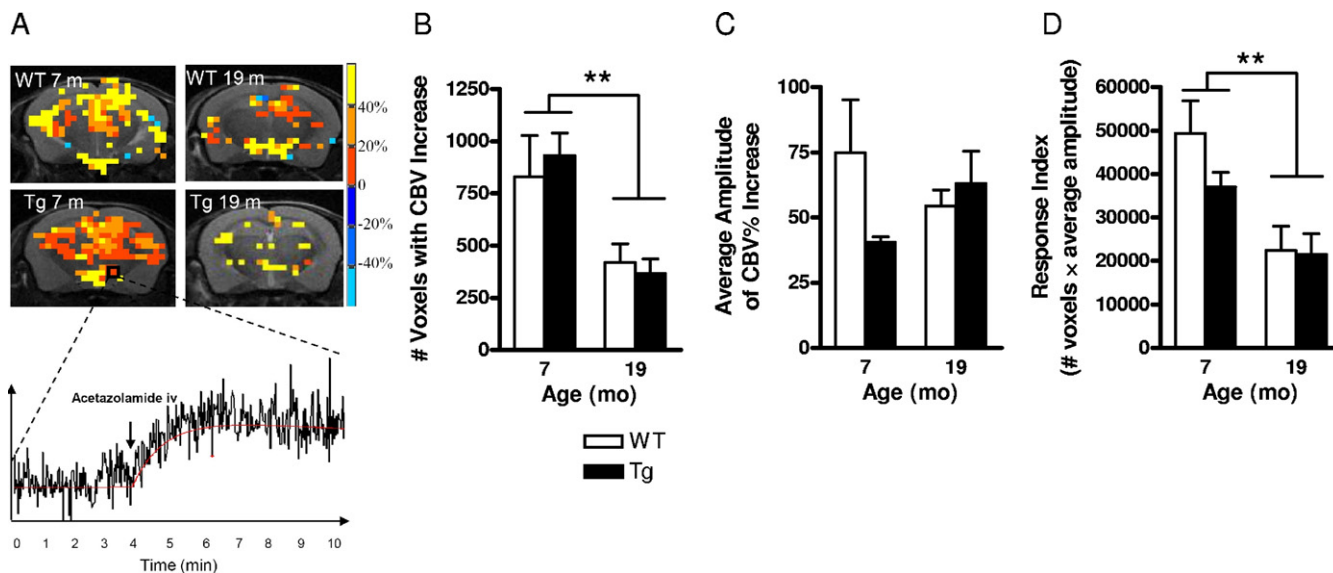


Fig. 4. Group average functional activation map and representative raw time course for cerebral blood volume (CBV)-based fMRI responses to acetazolamide administration (intravenous) is illustrated (A). The color bar on the right encodes the percentage signal change (CBV%) per voxel. Group comparison of functional magnetic resonance imaging (fMRI) CBV response to acetazolamide challenge between transgenic (Tg) and wild-type (WT) mice at 7 months and 19 months of age in terms of numbers of activated voxels with increased CBV (B), mean amplitude change of activated voxels (C), and response index (number of activated voxels) \times (average amplitude CBV% change of activated voxels) (D).

4. Discussion

In the present studies we report several key findings that challenge the utility of glucose metabolism in Tg2576 mice as a translatable model of AD and as a tool in target validation. Alzheimer's patients manifest specific and progressive reductions in cerebral glucose metabolism such that changes in the entorhinal cortex and hippocampus can differentiate individuals that convert from MCI to AD from those who remain MCI (Jagust, 2006). The largest reductions in CMRglu are observed in the posterior cingulate cortex (Jagust, 2006; Norfray and Provenzale, 2004). In contrast, our studies with Tg2576 mice demonstrated a global hypermetabolism as early as 3 months of age (data not shown) and confirmed again at 7 months of age. Furthermore, this hypermetabolism was associated with an elevation of taurine concentrations as revealed with proton magnetic resonance spectroscopy (MRS) (see supplementary material; also see Dedeoglu et al., 2004, and Marjanska et al., 2005). Using fMRI CBV we then determined that the integrity of the cerebral vascular compliance in 7-month-old Tg2576 vs. WT was intact. These data suggest that the Tg2576 mice have brain hypermetabolism, which cannot be accounted for by changes in vascular compliance but which may be due to a primary central nervous system (CNS) process related to amyloid hyperproduction. Taken together, these data suggest that the utility of the Tg2576 model may be limited to studying A β production and clearance mechanisms, rather than neuronal metabolism.

Imaging endpoints can be used as biomarkers to evaluate treatments that may slow or delay the disease process. They

can also be employed to evaluate the quality of animal models of the disease and improve the congruency or the most translatable endpoints from mice to patients (Day et al., 2008; Fox et al., 2005; Jack et al., 2003), thus providing new potential surrogate markers of AD processes that could be used to help clarify disease mechanisms and screen candidate treatments. The observation of hypermetabolism in young Tg2576 mice suggests that the Swedish mutation fails to capture CGU decreases as a marker of disease onset or severity.

One potential explanation for this result is that FDG-PET in mice is not sensitive enough to detect specific CGU changes in brain. Low resolution was speculated as the cause of finding no difference between transgenic and wild type animals in Tg2576 mice (~14 month) using FDG-PET (Kuntner et al., 2009). Niwa et al. (2002) published work utilizing 2-[¹⁴C]-deoxyglucose (DG) autoradiography which revealed a hypometabolism in Tg2576 mice at 2–3 months of age. The results from this report may imply that the autoradiographic method is a more sensitive tool than FDG-PET for investigating glucose utilization in mice. While the spatial resolution is clearly superior using autoradiography, there are reports that CGU via the PET method yields results consistent with those from autoradiography. Toyama et al. (2004) published a report demonstrating consistent results in quantitative CGU using a dual tracer ([¹⁸F]-FDG, 2-[¹⁴C]-DG), utilizing both FDG-PET and 2-DG autoradiography in mice (Toyama et al., 2004). Further, we have collected data in house using the same dual tracer in 17-month-old Tg2576 mice and showed a significant correlation in glucose utili-

zation using [^{18}F]-FDG and 2- [^{14}C]-DG in the same animals (unpublished data). We used the Invenio microPET in the current study, which bears similar spatial resolution but superior sensitivity to that of other commercial microPET systems (Visser et al., 2009), and, as demonstrated in Fig. 1, all defined regions of interest (ROIs) were far from facial glands which produce strong spill-over effects. Nevertheless, we acknowledge that some relatively small regions are subject to spill-over effects, e.g., effects from hippocampus to entorhinal cortex (Mirrione et al., 2007).

Other lines of AD transgenic mice have produced similar conflicting reports in terms of CGU. Several reports using autoradiography demonstrate that PDAPP and PSAPP mice are hypometabolic in specific brain regions, such as posterior cingulate cortex, suggesting potential congruency of glucose metabolism measures to AD (Mega et al., 1997; Mosconi, 2005). There has also been shown a highly significant, specific, and progressive reduction in FDG autoradiography in the posterior cingulate cortex of homozygous transgenic PDAPP mice overexpressing human mutant β -amyloid precursor protein (Reiman et al., 2000). The finding in this region was enticing as the rodent posterior cingulate cortex is potentially homologous to the human, subserving similar functions, such as spatial (Mantani et al., 2005; Vann et al., 2000) and associative/discriminative (Gabriel et al., 1987) learning. In contrast, Valla et al. (2008) showed by FDG autoradiography that PDAPP mice were significantly hypermetabolic in somatosensory cortex, CA1 region of hippocampus, and caudate putamen compared with WT mice, although there were regions demonstrating hypometabolism as well. Further, a recent report illustrated cerebral hypermetabolism in 14-month-old mice expressing both the Swedish and Indiana APP mutations (Nicolakakis et al., 2008).

Whereas several reports utilized a relative measure (normalizing the region of interest to a reference region, e.g., cerebellum) in order to minimize statistical variation in population-based data (Grunder, 2009), the use of such a reference region in Tg2576 mice is not appropriate as (1) these mice ubiquitously overexpress the Swedish APP transgene in the cerebellum, and (2) our data suggest that there is no true “unaffected” region with which to normalize the data when compared with wide type mice. Indeed, our data show that 7-month-old Tg mice have higher CGU in cerebellum than age-matched WT mice. Normalization to cerebellum would possibly cause an artifactual error due to incomparable baseline glucose uptake in the reference region. Further, Grunder (2009) demonstrated that if baseline glucose uptake differs in reference regions among treatment groups (even nonsignificantly), normalization of uptake may be misinterpreted. SUV, the widely applied clinical measure for FDG-PET studies, was therefore chosen as the outcome measure in this translational study.

The increased CGU seen in Tg2576 mice could be related to several factors, such as an increase in general basal

metabolic rate, reflecting increased APP expression, and potentially increased amyloid burden. For example, multiple studies have found that synthetic amyloid assemblies form both general membrane pores (Kayed et al., 2004) and more selective ion channels (Bhatia et al., 2000). The localization of $\text{A}\beta$ within mitochondria is consistent with this possibility (Atamna and Frey, 2007). The formation of membrane pores by assemblies of $\text{A}\beta$ may deplete the normal ionic gradients established by the sodium pump and other transporters, causing an increased demand for ionic pumping through Na-K ATPase or other ion transport systems. This activity uses roughly 20% of basal energy needs throughout the body, and as much as 60% of brain adenosine triphosphate (ATP) is used for this function (Clausen et al., 1991). These actions of $\text{A}\beta$ assemblies may increase energy demands in the brain and possibly elsewhere (e.g., fibroblasts; Etcheberrigaray et al., 2004), leading to increased basal metabolic rates.

Increased basal metabolism in the mammalian brain can be affected by hormone levels, age, sex, and genetic background (Eidelberg et al., 1991; Moe et al., 2007; Ronning et al., 2007). Additionally, increased activity and food intake in transgenic mice compared with controls could result in a hypermetabolic state (Morgan and Gordon, 2008; Vloeberghs et al., 2008). Differences in locomotor activity, however, cannot explain the increased CGU in our work (as mice were anesthetized during FDG uptake), and other factors such as age and sex were controlled in the current study. However, 2 plausible and relevant factors warrant further consideration: (1) overexpression of APP; and (2) excess $\text{A}\beta$ in Tg2576 mice. Although discriminating excess $\text{A}\beta$ from APP overexpression is not a trivial task, Ohno et al. (2004) successfully demonstrated that the BACE1 null mutation protected APP overexpressing mice from developing memory deficits, suggesting that accumulating $\text{A}\beta$ levels in APP mice were responsible for these effects (Ohno et al., 2004).

Another explanation for hypermetabolism is potential seizure activity related to increased $\text{A}\beta$ overexpression, as posited by Palop et al. (2007). The work by Palop and colleagues demonstrated that young mice expressing familial amyloid mutations show increased excitability and non-convulsive seizure activity via *in vivo* electrophysiology. The increased activity was seen in all portions of the cortex and in the hippocampus. While we did not investigate whether our Tg2576 mice demonstrated similar neuronal hyperactivity, this characteristic might account for the increased metabolism in the brain described in our work. Palop et al. did not investigate whether older mice exhibit the same nonconvulsive seizure activity as young mice, however, it is possible that compensatory mechanisms may arise to counteract the actions of increased $\text{A}\beta$ expression. Indeed, even in young mice, the authors describe changes in neuropeptide Y receptor expression and GABAergic transmission, which could arise due to the increased excitability

seen in this line. Whether these compensatory processes progress into older mice has not been evaluated, but may help to explain why the hypermetabolism detected in younger mice in our studies is not present when the animals reach older ages.

Although there is indirect evidence to support the above explanations, another consideration is necessary. It is well known that compensatory processes may take over the functions of a missing or overexpressed gene in knockouts or transgenic mice. This has been reviewed for models of energy homeostasis by Inui (2000). Therefore, caution needs to be exercised for the potential confounding factor of developmental compensation, as gene disruption or excess gene expression may perturb the organism and cause it to respond in a way to maintain its original biological organization (Inui, 2000). Previous reports have shown that young (4.5 and 11 months) Tg2576 mice show attrition of dendritic spine and arborization that worsens with age, but is indistinguishable from WT mice at 20 months (Lanz et al., 2003). These data, in conjunction with our current results, suggest a temporal correlation between cerebral hypermetabolism and loss of dendritic spine density, raising the possibility that cerebral hypermetabolism may serve a compensatory role.

It does not appear from our data that beta amyloid plaques are the cause of the hypermetabolism detected in Tg2576 mice. These mice do not demonstrate significant plaque pathology at 7 months of age (Callahan et al., 2001; Kawarabayashi et al., 2001) when they demonstrate high CGU in our FDG-PET study (see supplementary materials). At 19 months of age, when plaque burden is present (see supplementary materials), the Tg mice exhibited a CGU similar to WT mice. Further, the global effects we saw do not track with the severity of plaque burden in Tg mice. While we saw increased CGU in nearly all regions, plaque pathology is greatest in hippocampus and cortex. Hence, it is possible that the hypermetabolism detected in our study is due to soluble aggregates of beta amyloid rather than deposited plaques. At a minimum, it appears that the hypermetabolism is the result of the overexpression of the APP/Swe transgene.

There are several potential caveats to our interpretation that the CMRglu reductions seen in Tg2576 fail to mimic those associated with AD. Firstly, we did not observe a significant age-dependent decrease in CGU in WT animals. There are several potential explanations for this. The study did not employ a within-subjects design. The young and aged groups were from different cohorts of mice, but tested at the same time. As such, while controlling for the time of testing, the possibility exists that employing a within subjects approach could have been a more sensitive design to detect intra-animal changes in glucose. In addition, methodological considerations limited the number of brain regions that could be analyzed, unlike the studies conducted in rats, monkeys, and humans. Although advanced microPET

systems have been successfully applied in mouse imaging studies (Chatziioannou et al., 1999; Phelps, 2000; Tai et al., 2003; Yang et al., 2004), spillover and partial volume effects are still challenging for quantifying radioactivity from small brain regions. A recent microPET mouse study failed to detect a regional decrease in glucose metabolism compared with autoradiography in 13–15-month-old Tg2576 mice (Kuntner et al., 2009), suggesting difficulties in volume definition and radioactivity measurement for small VOIs due to a partial volume effect — an intrinsic limitation for mouse PET imaging (Mirrione et al., 2007). Therefore only VOIs larger than 5 mm³ were included in the current study data analysis, because 5 mm³ volume was reported to be less susceptible to spill-over effects using a microPET R4 tomograph (Concorde Microsystems, Knoxville, TN, USA) (Mirrione et al., 2007). Inveon microPET was employed in the current study, which bears similar spatial resolution but superior sensitivity to that of other commercial microPET systems (Visser et al., 2009), and, as demonstrated in Fig. 1, all defined regions of interest (ROIs) were far from facial glands which produce strong spill-over effects. However, whether VOIs larger than 5 mm³ are free from partial volume effect is under debate. A recent investigation on the advanced microPET system (Constantinescu and Mukherjee, 2009) indicates that 9 mm³ VOI may avoid a partial volume effect (Phelps, 2006). Although a 5 mm³ volume was chosen in the current study as the minimal brain structure size to be analyzed, the majority of our regions were larger than 9 mm³ (with the exception of the perirhinal and entorhinal cortices). Importantly, we saw the same transgene effect (i.e., hypermetabolism) in 7-month-old Tg mice regardless of the size of the VOI.

A second potential explanation is that the Tg2576 mouse represents a pre-AD state. Although there is no evidence to our knowledge that resting-state cerebral hypermetabolism exists in either AD or in any pre-AD state, increases in task-induced blood oxygenation level dependent (BOLD) signals or blood flow have been seen in medial temporal structures of MCI patients (Alsop et al., 2008; Dickerson et al., 2005). In addition, cerebral hypermetabolism has been reported in patients with Down's syndrome in an activation task (Haier et al., 2008) and at rest (Lengyel et al., 2006). The latter finding may reflect a stronger congruency between CGU in Down's syndrome patients (who overproduce amyloid beta) and Tg2576 mice than between AD patients and Tg 2576 mice.

In the present studies, differences were observed between WT and Tg animals under the same anesthetic conditions. Anesthesia is generally considered a caveat to such studies. Ketamine, a noncompetitive NMDA receptor antagonist, has been characterized as both a psychoactive or anesthetic substance depending on the dose of the drug used (Greene, 2001; Gunduz-Bruce, 2009). The psychoactive doses of the drug have been shown to increase blood oxygenation level and blood flow across several regions of the

brain in rodent, non-human primate, and human central nervous system (CNS) (Burdett et al., 1995; Leopold et al., 2002; Littlewood et al., 2006; Werner et al., 1990). Our present studies employed ketamine at anesthetic levels, which have been demonstrated to show decreased cerebral blood flow (CBF) (Lowry and Fillenz, 2001) and BOLD (in-house data being prepared for journal submission). Our multimodal imaging data converge to the conclusion of a hypermetabolic state in young Tg2576 mice.

Our CGU study was completed under anesthesia with combined ketamine and medetomidine. One concern for glucose utilization is the decrease in body temperature that accompanies anesthesia with ketamine (Ulugol et al., 2000). Pilot work in our laboratory (unpublished data) has demonstrated that WT and Tg mice do not differ in the hypothermic response to ketamine, suggesting that the hypothermic response is not the sole mediator of the increased glucose uptake in Tg mice found in the current work. Additionally, the majority of the glucose uptake in the brain after an intravenous bolus of FDG occurs within 5 minutes of injection (see Fig. 2). Hence, while hypothermia increases glucose uptake in heat-generating tissue such as muscle and brown fat, the early uptake of FDG is likely minimally affected by this, as peak hypothermic effects of ketamine occurred at 30 minutes postinjection (Ulugol et al., 2000). Additionally, even when given 30 minutes prior to the administration of FDG, ketamine anesthesia does not show significant alternation of global glucose uptake when compared with conscious stage in rats (Matsumura et al., 2003).

Imaging nonhuman primate and rat in the awake state is time-consuming and challenging due to the training period required to acclimate animals to the imaging environment and scanner noise, especially for fMRI studies. As a consequence, the majority of animal fMRI studies are conducted under anesthesia (King et al., 2005). Feasibility of imaging conscious mice has not been reported as imaging a mouse is more challenging than that of a rat (Myers and Hume, 2002). However, it is known that many anesthetic agents can reduce and suppress neurovascular coupling (King et al., 2005) and relatively few anesthetic agents preserve meaningful fMRI signals. This is particularly true for BOLD fMRI signals, which are routinely utilized in awake subjects in the clinic (Van der Linden et al., 2007). However, we feel that it is unlikely that our core findings are significantly influenced by anesthesia. Firstly, we used medetomidine, an α_2 -adrenoreceptor agonist, as the anesthetic agent, which has been demonstrated to preserve fMRI signals in rats and birds and can be used for longitudinal studies (Van der Linden et al., 2007; Weber et al., 2006). Secondly, an MRS study we completed demonstrating trends for higher taurine/total creatine ratios in APP transgenic mice under medetomidine anesthesia (see supplementary materials) are consistent with other reports using isoflurane and halothane as anesthetic agents (Dedeoglu et al., 2004; Marjanska et al., 2005). CBV decreases observed in a

mouse fMRI study following $A\beta_{1-40}$ (but not inverse sequence $A\beta_{40-1}$) challenge under medetomidine anesthesia (Luo et al., 2008) are similar to $A\beta_{1-40}$ induced vascular dysfunction under awake conditions (Luo et al., 2008). Taken together, it is unlikely that medetomidine anesthesia confounds our imaging findings with PET and fMRI.

In summary, advances in clinical neuroimaging are enabling early detection of dementias such as AD, often before clinical symptoms are apparent, as well as the possibility of tracking disease progression (Jagust and Eberling, 1991). Consequently, translational imaging represents an attractive approach to developing new disease-modifying therapies by reducing the inherent risk associated with advancing new drugs to complex clinical trials (Fox et al., 2005; Jack et al., 2003; Teipel et al., 2006). Unfortunately, few studies have been conducted in this challenging area. The present study aimed to address this gap, using high-resolution animal [18 F]-FDG-PET in conjunction with functional MRI in an APP transgenic mouse model (Tg2576) to assess brain metabolism and vascular compliance. The unexpected findings of hypermetabolism in Tg2576 mice run counter to those anticipated based on clinical experience in Alzheimer's patients. Therefore, the Tg2576 model fails to recapitulate a major hallmark of AD and this suggests significant limitations in using the model to predict clinical outcome.

Disclosure statement

All authors are employees of Abbott Laboratories, except Sarah Mudd who works at School of Pharmacy, University of Wisconsin.

All experiments were conducted in accordance with Abbott Institutional Animal Care and Use Committee and National Institutes of Health Guide for Care and Use of Laboratory Animals guidelines in facilities accredited by the Association for the Assessment and Accreditation of Laboratory Animal Care.

Acknowledgements

The authors extend their gratitude to Drs. Wolfgang Ebert, Bernd Misselwitz, and Hans Bauer (Bayer Schering Health Care, Germany) for providing SH U 555 C contrast agent. Also, special thanks to Edward Olejniczak for expert technical assistance and Chih-Liang Chin for helpful comments on the manuscript.

Source of the study funding comes from Abbott Laboratories.

Appendix. Supplementary data

Supplementary data associated with this article can be found, in the online version, at [doi:10.1016/j.neurobiolaging.2010.08.005](https://doi.org/10.1016/j.neurobiolaging.2010.08.005).

References

- Alexander, G.E., Chen, K., Pietrini, P., Rapoport, S.I., Reiman, E.M., 2002. Longitudinal PET evaluation of cerebral metabolic decline in dementia: a potential outcome measure in Alzheimer's disease treatment studies. *Am. J. Psychiatry* 159, 738–745.
- Alsop, D.C., Casement, M., de Bazelaire, C., Fong, T., Press, D.Z., 2008. Hippocampal hyperperfusion in Alzheimer's disease. *Neuroimage* 42, 1267–1274.
- Atamna, H., Frey, W.H., 2nd, 2007. Mechanisms of mitochondrial dysfunction and energy deficiency in Alzheimer's disease. *Mitochondrion* 7, 297–310.
- Bhatia, R., Lin, H., Lal, R., 2000. Fresh and globular amyloid beta protein (1–42) induces rapid cellular degeneration: evidence for AbetaP channel-mediated cellular toxicity. *FASEB J.* 14, 1233–1243.
- Boellaard, R., van Lingen, A., Lammertsma, A.A., 2001. Experimental and clinical evaluation of iterative reconstruction (OSEM) in dynamic PET: quantitative characteristics and effects on kinetic modeling. *J. Nucl. Med.* 42, 808–817.
- Burdett, N.G., Menon, D.K., Carpenter, T.A., Jones, J.G., Hall, L.D., 1995. Visualisation of changes in regional cerebral blood flow (rCBF) produced by ketamine using long TE gradient-echo sequences: preliminary results. *Magn. Reson. Imaging* 13, 549–553.
- Callahan, M.J., Lipinski, W.J., Bian, F., Durham, R.A., Pack, A., Walker, L.C., 2001. Augmented senile plaque load in aged female beta-amyloid precursor protein-transgenic mice. *Am. J. Pathol.* 158, 1173–1177.
- Chatzioannou, A.F., Cherry, S.R., Shao, Y., Silverman, R.W., Meadors, K., Farquhar, T.H., Pedarsani, M., Phelps, M.E., 1999. Performance evaluation of microPET: a high-resolution lutetium oxorthosilicate PET scanner for animal imaging. *J. Nucl. Med.* 40, 1164–1175.
- Clausen, T., Van Hardevelde, C., Everts, M.E., 1991. Significance of cation transport in control of energy metabolism and thermogenesis. *Physiol. Res.* 71, 733–774.
- Constantinescu, C.C., Mukherjee, J., 2009. Performance evaluation of an Inveon PET preclinical scanner. *Phys. Med. Biol.* 54, 2885–2899.
- Cox, R.W., 1996. AFNI: software for analysis and visualization of functional magnetic resonance neuroimages. *Comput. Biomed. Res.* 29, 162–173.
- Day, M., Balci, F., Wan, H.I., Fox, G.B., Rutkowski, J.L., Feuerstein, G., 2008. Cognitive endpoints as disease biomarkers: optimizing the congruency of preclinical models to the clinic. *Curr. Opin. Investig. Drugs* 9, 696–706.
- de Leon, M.J., Convit, A., Wolf, O.T., Tarshish, C.Y., DeSanti, S., Rusinek, H., Tsui, W., Kandil, E., Scherer, A.J., Roche, A., Imossi, A., Thorn, E., Bobinski, M., Caraos, C., Lesbre, P., Schlyer, D., Poirier, J., Reisberg, B., Fowler, J., 2001. Prediction of cognitive decline in normal elderly subjects with 2-[(18F)fluoro-2-deoxy-D-glucose/positron-emission tomography (FDG/PET). *Proc. Natl. Acad. Sci. U. S. A.* 98, 10966–10971.
- Dedeoglu, A., Choi, J.K., Cormier, K., Kowall, N.W., Jenkins, B.G., 2004. Magnetic resonance spectroscopic analysis of Alzheimer's disease mouse brain that express mutant human APP shows altered neurochemical profile. *Brain Res.* 1012, 60–65.
- Dickerson, B.C., Salat, D.H., Greve, D.N., Chua, E.F., Rand-Giovannetti, E., Rentz, D.M., Bertram, L., Mullin, K., Tanzi, R.E., Blacker, D., Albert, M.S., Sperling, R.A., 2005. Increased hippocampal activation in mild cognitive impairment compared to normal aging and AD. *Neurology* 65, 404–411.
- Dickerson, B.C., Sperling, R.A., 2005. Neuroimaging biomarkers for clinical trials of disease-modifying therapies in Alzheimer's disease. *NeuroRx* 2, 348–360.
- Eidelberg, D., Dhawan, V., Moeller, J.R., Sidtis, J.J., Ginos, J.Z., Strother, S.C., Cederbaum, J., Greene, P., Fahn, S., Powers, J.M., 1991. The metabolic landscape of cortico-basal ganglionic degeneration: regional asymmetries studied with positron emission tomography. *J. Neurol. Neurosurg. Psychiatry* 54, 856–862.
- Etcheberrigaray, R., Tan, M., Dewachter, I., Kuiperi, C., Van der Auwera, I., Wera, S., Qiao, L., Bank, B., Nelson, T.J., Kozikowski, A.P., Van Leuven, F., Alkon, D.L., 2004. Therapeutic effects of PKC activators in Alzheimer's disease transgenic mice. *Proc. Natl. Acad. Sci. U. S. A.* 101, 11141–11146.
- Fox, N.C., Black, R.S., Gilman, S., Rossor, M.N., Griffith, S.G., Jenkins, L., Koller, M., 2005. Effects of Abeta immunization (AN1792) on MRI measures of cerebral volume in Alzheimer disease. *Neurology* 64, 1563–1572.
- Gabriel, M., Sparenborg, S.P., Stolar, N., 1987. Hippocampal control of cingulate cortical and anterior thalamic information processing during learning in rabbits. *Exp. Brain Res.* 67, 131–152.
- Graham, G.D., Zhong, J., Petroff, O.A., Constable, R.T., Prichard, J.W., Gore, J.C., 1994. BOLD MRI monitoring of changes in cerebral perfusion induced by acetazolamide and hypercarbia in the rat. *Magn. Reson. Med.* 31, 557–560.
- Greene, R., 2001. Circuit analysis of NMDAR hypofunction in the hippocampus, in vitro, and psychosis of schizophrenia. *Hippocampus* 11, 569–577.
- Grunder, G., 2009. "Absolute" or "relative": choosing the right outcome measure in neuroimaging. *Neuroimage* 45, 258–259.
- Gunduz-Bruce, H., 2009. The acute effects of NMDA antagonism: from the rodent to the human brain. *Brain Res. Rev.* 60, 279–286.
- Haier, R.J., Head, K., Head, E., Lott, I.T., 2008. Neuroimaging of individuals with Down's syndrome at-risk for dementia: evidence for possible compensatory events. *Neuroimage* 39, 1324–1332.
- Hsiao, K., 1998. Transgenic mice expressing Alzheimer amyloid precursor proteins. *Exp. Gerontol.* 33, 883–889.
- Hsiao, K., Chapman, P., Nilsen, S., Eckman, C., Harigaya, Y., Younkin, S., Yang, F., Cole, G., 1996. Correlative memory deficits, Abeta elevation, and amyloid plaques in transgenic mice. *Science* 274, 99–102.
- Hudson, H.M., Larkin, R.S., 1994. Accelerated image reconstruction using ordered subsets of projection data. *IEEE Trans. Med. Imaging* 13, 601–609.
- Inui, A., 2000. Transgenic study of energy homeostasis equation: implications and confounding influences. *FASEB J.* 14, 2158–2170.
- Irizarry, M.C., McNamara, M., Fedorchak, K., Hsiao, K., Hyman, B.T., 1997. APPSw transgenic mice develop age-related A beta deposits and neuropil abnormalities, but no neuronal loss in CA1. *J. Neuropathol. Exp. Neurol.* 56, 965–973.
- Jack, C.R., Jr, Slomkowski, M., Gracon, S., Hoover, T.M., Felmlee, J.P., Stewart, K., Xu, Y., Shiung, M., O'Brien, P.C., Cha, R., Knopman, D., Petersen, R.C., 2003. MRI as a biomarker of disease progression in a therapeutic trial of milameline for AD. *Neurology* 60, 253–260.
- Jacobsen, J.S., Wu, C.C., Redwine, J.M., Comery, T.A., Arias, R., Bowlby, M., Martone, R., Morrison, J.H., Pangalos, M.N., Reinhart, P.H., Bloom, F.E., 2006. Early-onset behavioral and synaptic deficits in a mouse model of Alzheimer's disease. *Proc. Natl. Acad. Sci. U. S. A.* 103, 5161–5166.
- Jagust, W., 2006. Positron emission tomography and magnetic resonance imaging in the diagnosis and prediction of dementia. *Alzheimers Dement.* 2, 36–42.
- Jagust, W.J., Eberling, J.L., 1991. MRI, CT, SPECT, PET: their use in diagnosing dementia. *Geriatrics* 46, 28–35.
- Kawarabayashi, T., Younkin, L.H., Saido, T.C., Shoji, M., Ashe, K.H., Younkin, S.G., 2001. Age-dependent changes in brain, CSF, and plasma amyloid (beta) protein in the Tg2576 transgenic mouse model of Alzheimer's disease. *J. Neurosci.* 21, 372–381.
- Kayed, R., Sokolov, Y., Edmonds, B., McIntire, T.M., Milton, S.C., Hall, J.E., Glabe, C.G., 2004. Permeabilization of lipid bilayers is a common conformation-dependent activity of soluble amyloid oligomers in protein misfolding diseases. *J. Biol. Chem.* 279, 46363–46366.
- King, J.A., Garelick, T.S., Brevard, M.E., Chen, W., Messenger, T.L., Duong, T.Q., Ferris, C.F., 2005. Procedure for minimizing stress for fMRI studies in conscious rats. *J. Neurosci. Methods* 148, 154–160.

- Klunk, W.E., Lopresti, B.J., Ikonovic, M.D., Lefterov, I.M., Kolamova, R.P., Abrahamson, E.E., Debnath, M.L., Holt, D.P., Huang, G.F., Shao, L., DeKosky, S.T., Price, J.C., Mathis, C.A., 2005. Binding of the positron emission tomography tracer Pittsburgh compound B reflects the amount of amyloid-beta in Alzheimer's disease brain but not in transgenic mouse brain. *J. Neurosci.* 25, 10598–10606.
- Kuntner, C., Kesner, A.L., Bauer, M., Kremslehner, R., Wanek, T., Mandler, M., Karch, R., Stanek, J., Wolf, T., Muller, M., Langer, O., 2009. Limitations of small animal PET imaging with [18F]FDDNP and FDG for quantitative studies in a transgenic mouse model of Alzheimer's disease. *Mol. Imaging Biol.* 11, 236–240.
- Lanz, T.A., Carter, D.B., Merchant, K.M., 2003. Dendritic spine loss in the hippocampus of young PDAPP and Tg2576 mice and its prevention by the ApoE2 genotype. *Neurobiol. Dis.* 13, 246–253.
- Leahy, R.M., Qi, J., 2000. Statistical approaches in quantitative positron emission tomography. *Stat. Comput.* 10, 147–165.
- Lengyel, Z., Balogh, E., Emri, M., Szikszai, E., Kollar, J., Sikula, J., Esik, O., Tron, L., Olah, E., 2006. Pattern of increased cerebral FDG uptake in Down syndrome patients. *Pediatr. Neurol.* 34, 270–275.
- Leopold, D.A., Plettenberg, H.K., Logothetis, N.K., 2002. Visual processing in the ketamine-anesthetized monkey. Optokinetic and blood oxygenation level-dependent responses. *Exp. Brain Res.* 143, 359–372.
- Littlewood, C.L., Cash, D., Dixon, A.L., Dix, S.L., White, C.T., O'Neill, M.J., Tricklebank, M., Williams, S.C., 2006. Using the BOLD MR signal to differentiate the stereoisomers of ketamine in the rat. *Neuroimage* 32, 1733–1746.
- Lowry, J.P., Fillenz, M., 2001. Real-time monitoring of brain energy metabolism in vivo using microelectrochemical sensors: the effects of anesthesia. *Bioelectrochemistry* 54, 39–47.
- Luo, F., Seifert, T.R., Edalji, R., Loebbert, R.W., Hradil, V.P., Harlan, J., Schmidt, M., Nimmrich, V., Cox, B.F., Fox, G.B., 2008. Non-invasive characterization of beta-amyloid(1–40) vasoactivity by functional magnetic resonance imaging in mice. *Neuroscience* 155, 263–269.
- Luo, F., Wu, G., Li, Z., Li, S.J., 2003. Characterization of effects of mean arterial blood pressure induced by cocaine and cocaine methiodide on BOLD signals in rat brain. *Magn. Reson. Med.* 49, 264–270.
- Luo, F., Xi, Z.X., Wu, G., Liu, C., Gardner, E.L., Li, S.J., 2004. Attenuation of brain response to heroin correlates with the reinstatement of heroin-seeking in rats by fMRI. *Neuroimage* 22, 1328–1335.
- Mandeville, J.B., Marota, J.J., Kosofsky, B.E., Keltner, J.R., Weissleder, R., Rosen, B.R., Weisskoff, R.M., 1998. Dynamic functional imaging of relative cerebral blood volume during rat forepaw stimulation. *Magn. Reson. Med.* 39, 615–624.
- Mantani, T., Okamoto, Y., Shirao, N., Okada, G., Yamawaki, S., 2005. Reduced activation of posterior cingulate cortex during imagery in subjects with high degrees of alexithymia: a functional magnetic resonance imaging study. *Biol. Psychiatry* 57, 982–990.
- Marjanska, M., Curran, G.L., Wengenack, T.M., Henry, P.G., Bliss, R.L., Poduslo, J.F., Jack, C.R., Jr, Ugurbil, K., Garwood, M., 2005. Monitoring disease progression in transgenic mouse models of Alzheimer's disease with proton magnetic resonance spectroscopy. *Proc. Natl. Acad. Sci. U. S. A.* 102, 11906–11910.
- Matsumura, A., Mizokawa, S., Tanaka, M., Wada, Y., Nozaki, S., Nakamura, F., Shiomi, S., Ochi, H., Watanabe, Y., 2003. Assessment of microPET performance in analyzing the rat brain under different types of anesthesia: comparison between quantitative data obtained with microPET and ex vivo autoradiography. *Neuroimage* 20, 2040–2050.
- McGowan, E., Eriksen, J., Hutton, M., 2006. A decade of modeling Alzheimer's disease in transgenic mice. *Trends Genet.* 22, 281–289.
- Mega, M.S., Chen, S.S., Thompson, P.M., Woods, R.P., Karaca, T.J., Tiwari, A., Vinters, H.V., Small, G.W., Toga, A.W., 1997. Mapping histology to metabolism: coregistration of stained whole-brain sections to premortem PET in Alzheimer's disease. *Neuroimage* 5, 147–153.
- Miller, G., 2009. Alzheimer's biomarker initiative hits its stride. *Science* 326, 386–389.
- Mirrione, M.M., Schiffer, W.K., Fowler, J.S., Alexoff, D.L., Dewey, S.L., Tsirka, S.E., 2007. A novel approach for imaging brain-behavior relationships in mice reveals unexpected metabolic patterns during seizures in the absence of tissue plasminogen activator. *Neuroimage* 38, 34–42.
- Moe, B., Angelier, F., Bech, C., Chastel, O., 2007. Is basal metabolic rate influenced by age in a long-lived seabird, the snow petrel? *J. Exp. Biol.* 210, 3407–3414.
- Morgan, D., Gordon, M.N., 2008. Amyloid, hyperactivity, and metabolism: theoretical comment on Vloeberghs et al. *Behav. Neurosci.* 122, 730–732.
- Mosconi, L., 2005. Brain glucose metabolism in the early and specific diagnosis of Alzheimer's disease. FDG-PET studies in MCI and AD. *Eur. J. Nucl. Med. Mol. Imaging* 32, 486–510.
- Mueggler, T., Sturchler-Pierrat, C., Baumann, D., Rausch, M., Staufenbiel, M., Rudin, M., 2002. Compromised hemodynamic response in amyloid precursor protein transgenic mice. *J. Neurosci.* 22, 7218–7224.
- Myers, R., Hume, S., 2002. Small animal PET. *Eur. Neuropsychopharmacol.* 12, 545–555.
- Nicolakakis, N., Aboukassim, T., Ongali, B., Lecrux, C., Fernandes, P., Rosa-Neto, P., Tong, X.K., Hamel, E., 2008. Complete rescue of cerebrovascular function in aged Alzheimer's disease transgenic mice by antioxidants and pioglitazone, a peroxisome proliferator-activated receptor gamma agonist. *J. Neurosci.* 28, 9287–9296.
- Niwa, K., Kazama, K., Younkin, S.G., Carlson, G.A., Iadecola, C., 2002. Alterations in cerebral blood flow and glucose utilization in mice overexpressing the amyloid precursor protein. *Neurobiol. Dis.* 9, 61–68.
- Norfray, J.F., Provenzale, J.M., 2004. Alzheimer's disease: neuropathologic findings and recent advances in imaging. *AJR Am. J. Roentgenol.* 182, 3–13.
- Ohno, M., Sametsky, E.A., Younkin, L.H., Oakley, H., Younkin, S.G., Citron, M., Vassar, R., Disterhoft, J.F., 2004. BACE1 deficiency rescues memory deficits and cholinergic dysfunction in a mouse model of Alzheimer's disease. *Neuron* 41, 27–33.
- Palop, J.J., Chin, J., Roberson, E.D., Wang, J., Thwin, M.T., Bien-Ly, N., Yoo, J., Ho, K.O., Yu, G.Q., Kreitzer, A., Finkbeiner, S., Noebels, J.L., Mucke, L., 2007. Aberrant excitatory neuronal activity and compensatory remodeling of inhibitory hippocampal circuits in mouse models of Alzheimer's disease. *Neuron* 55, 697–711.
- Phelps, M.E., 2000. Inaugural article: positron emission tomography provides molecular imaging of biological processes. *Proc. Natl. Acad. Sci. U. S. A.* 97, 9226–9233.
- Phelps, M.E. (Ed.), 2006. *PET Physics, Instrumentation, and Scanners*. Springer, New York.
- Potkin, S.G., Anand, R., Fleming, K., Alva, G., Keator, D., Carreon, D., Messina, J., Wu, J.C., Hartman, R., Fallon, J.H., 2001. Brain metabolic and clinical effects of rivastigmine in Alzheimer's disease. *Int. J. Neuropsychopharmacol.* 4, 223–230.
- Reiman, E.M., Chen, K., Alexander, G.E., Caselli, R.J., Bandy, D., Osborne, D., Saunders, A.M., Hardy, J., 2005. Correlations between apolipoprotein E epsilon4 gene dose and brain-imaging measurements of regional hypometabolism. *Proc. Natl. Acad. Sci. U. S. A.* 102, 8299–8302.
- Reiman, E.M., Uecker, A., Gonzalez-Lima, F., Minear, D., Chen, K., Callaway, N.L., Berndt, J.D., Games, D., 2000. Tracking Alzheimer's disease in transgenic mice using fluorodeoxyglucose autoradiography. *Neuroreport* 11, 987–991.
- Roberson, E.D., Mucke, L., 2006. 100 years and counting: prospects for defeating Alzheimer's disease. *Science* 314, 781–784.
- Ronning, B., Jensen, H., Moe, B., Bech, C., 2007. Basal metabolic rate: heritability and genetic correlations with morphological traits in the zebra finch. *J. Evol. Biol.* 20, 1815–1822.
- Spires, T.L., Hyman, B.T., 2005. Transgenic models of Alzheimer's disease: learning from animals. *NeuroRx* 2, 423–437.
- Stein, E.A., 2001. fMRI: a new tool for the in vivo localization of drug actions in the brain. *J. Anal. Toxicol.* 25, 419–424.

- Tai, Y.C., Chatziioannou, A.F., Yang, Y., Silverman, R.W., Meadors, K., Siegel, S., Newport, D.F., Stichel, J.R., Cherry, S.R., 2003. MicroPET. II: design, development and initial performance of an improved microPET scanner for small-animal imaging. *Phys. Med. Biol.* 48, 1519–1537.
- Teipel, S.J., Drzezga, A., Bartenstein, P., Moller, H.J., Schwaiger, M., Hampel, H., 2006. Effects of donepezil on cortical metabolic response to activation during (18)FDG-PET in Alzheimer's disease: a double-blind cross-over trial. *Psychopharmacology* 187, 86–94.
- Thal, L.J., Kantarci, K., Reiman, E.M., Klunk, W.E., Weiner, M.W., Zetterberg, H., Galasko, D., Pratico, D., Griffin, S., Schenk, D., Siemers, E., 2006. The role of biomarkers in clinical trials for Alzheimer disease. *Alzheimer Dis. Assoc. Disord.* 20, 6–15.
- Thie, J.A., 2004. Understanding the standardized uptake value, its methods, and implications for usage. *J. Nucl. Med.* 45, 1431–1434.
- Toyama, H., Ichise, M., Liow, J.S., Modell, K.J., Vines, D.C., Esaki, T., Cook, M., Seidel, J., Sokoloff, L., Green, M.V., Innis, R.B., 2004. Absolute quantification of regional cerebral glucose utilization in mice by 18F-FDG small animal PET scanning and 2-14C-DG autoradiography. *J. Nucl. Med.* 45, 1398–1405.
- Ulugol, A., Dost, T., Dokmeci, D., Akpolat, M., Karadag, C.H., Dokmeci, I., 2000. Involvement of NMDA receptors and nitric oxide in the thermoregulatory effect of morphine in mice. *J. Neural Transm.* 107, 515–521.
- Valla, J., Gonzalez-Lima, F., Reiman, E.M., 2008. FDG autoradiography reveals developmental and pathological effects of mutant amyloid in PDAPP transgenic mice. *Int. J. Dev. Neurosci.* 26, 253–258.
- Van der Linden, A., Van Camp, N., Ramos-Cabrer, P., Hoehn, M., 2007. Current status of functional MRI on small animals: application to physiology, pathophysiology, and cognition. *NMR Biomed.* 20, 522–545.
- Vann, S.D., Brown, M.W., Aggleton, J.P., 2000. Fos expression in the rostral thalamic nuclei and associated cortical regions in response to different spatial memory tests. *Neuroscience* 101, 983–991.
- Visser, E.P., Disselhorst, J.A., Brom, M., Laverman, P., Gotthardt, M., Oyen, W.J., Boerman, O.C., 2009. Spatial resolution and sensitivity of the Inveon small-animal PET scanner. *J. Nucl. Med.* 50, 139–147.
- Vloeberghs, E., Van Dam, D., Franck, F., Serroyen, J., Geert, M., Staufenbiel, M., De Deyn, P.P., 2008. Altered ingestive behavior, weight changes, and intact olfactory sense in an APP overexpression model. *Behav. Neurosci.* 122, 491–497.
- Vorstrup, S., Henriksen, L., Paulson, O.B., 1984. Effect of acetazolamide on cerebral blood flow and cerebral metabolic rate for oxygen. *J. Clin. Invest.* 74, 1634–1639.
- Weber, R., Ramos-Cabrer, P., Wiedermann, D., van Camp, N., Hoehn, M., 2006. A fully noninvasive and robust experimental protocol for longitudinal fMRI studies in the rat. *Neuroimage* 29, 1303–1310.
- Werner, C., Kochs, E., Rau, M., Blanc, I., Am Esch, J.S., 1990. Dose-dependent blood flow velocity changes in the Basal cerebral arteries following low-dose ketamine. *J. Neurosurg. Anesthesiol.* 2, 86–91.
- Westerman, M.A., Cooper-Blacketer, D., Mariash, A., Kotilinek, L., Kawarabayashi, T., Younkin, L.H., Carlson, G.A., Younkin, S.G., Ashe, K.H., 2002. The relationship between Abeta and memory in the Tg2576 mouse model of Alzheimer's disease. *J. Neurosci.* 22, 1858–1867.
- Yang, Y., Tai, Y.C., Siegel, S., Newport, D.F., Bai, B., Li, Q., Leahy, R.M., Cherry, S.R., 2004. Optimization and performance evaluation of the microPET II scanner for in vivo small-animal imaging. *Phys. Med. Biol.* 49, 2527–2545.